

Research Article

Open Access



Liquid metal-based dynamic conformal electrodes

Xiaotong Liu^{1,*}, Chunxue Wan^{2,*}, Jiaping Liu^{3,*}, Hui Xu¹, Yubing Liu², Yi Liu⁴, Yanqing Liu¹, Jing Liu², Hongzhang Wang^{5,6}, Haojun Fan^{1,*}, Rui Guo^{2,3,*}

¹School of Disaster and Emergency Medicine, Tianjin University, Tianjin 300072, China.

²State Key Laboratory of Cryogenic Science and Technology, Technical Institute of Physics and Chemistry, Chinese Academy of Sciences, Beijing 100190, China.

³School of Precision Instrument and Opto-Electronics Engineering, Tianjin University, Tianjin 300072, China.

⁴Key Laboratory for Biomechanics and Mechanobiology of the Ministry of Education, School of Engineering Medicine, Beihang University, Beijing 100191, China.

⁵Institute of Materials Research & Center of Double Helix, Shenzhen International Graduate School, Tsinghua University, Shenzhen 518055, Guangdong, China.

⁶The Key Laboratory of Bionic Engineering (Ministry of Education), Jilin University, Changchun 130022, Jilin, China.

*Authors contributed equally.

Correspondence to: Haojun Fan, School of Disaster and Emergency Medicine, Tianjin University, No. 92 Weijin Road, Tianjin 300072, China. E-mail: fanhj@tju.edu.cn; Rui Guo, State Key Laboratory of Cryogenic Science and Technology, Technical Institute of Physics and Chemistry, Chinese Academy of Sciences, No. 29 Zhongguancun East Road, Haidian District, Beijing 100190, China. E-mail: guorui@mail.ipc.ac.cn

How to cite this article: Liu, X.; Wan, C.; Liu, J.; Xu, H.; Liu, Y.; Liu, Y.; Liu, Y.; Liu, J.; Wang, H.; Fan, H.; Guo, R. Liquid metal-based dynamic conformal electrodes. *Soft Sci.* 2025, 5, 34. <https://dx.doi.org/10.20517/ss.2025.16>

Received: 29 Apr 2025 **First Decision:** 10 Jun 2025 **Revised:** 30 Jun 2025 **Accepted:** 1 Jul 2025 **Published:** 18 Jul 2025

Academic Editor: Young Min Song **Copy Editor:** Pei-Yun Wang **Production Editor:** Pei-Yun Wang

Abstract

Electronic skin has increasingly diverse applications in health monitoring, disease diagnosis, rehabilitation therapy, and human-machine interaction. However, most electronic skin devices struggle to maintain stable performance and adhesion under complex conditions involving high body acceleration and sweat. To address these issues, we present a dynamic conformal electrode based on liquid metal, fabricated by coating the semi-liquid metal (SLM) with high conductivity of 9.0×10^6 S/m and low fluidity onto polyborosiloxane (PBS) exhibiting frequency-responsive rheological properties. The gradual deformation of PBS enables SLM to compress into microscopic skin wrinkles while avoiding hair interference. This dynamic conformal electrode can withstand significant deformation exceeding 1,000%, while also increasing the skin contact area, leading to a lower skin contact impedance of 0.1 M Ω at 1,000 Hz and improved interfacial adhesion, maintaining robust skin adhesion for over 7 days. This study demonstrates the capability of the conformal electrode to conduct long-term monitoring of electrocardiogram, electromyogram, and electroencephalogram signals in areas with rough textures, large skin deformation, and dense hair, enabling continuous dynamic monitoring of human health information. The findings highlight its broad



© The Author(s) 2025. **Open Access** This article is licensed under a Creative Commons Attribution 4.0 International License (<https://creativecommons.org/licenses/by/4.0/>), which permits unrestricted use, sharing, adaptation, distribution and reproduction in any medium or format, for any purpose, even commercially, as long as you give appropriate credit to the original author(s) and the source, provide a link to the Creative Commons license, and indicate if changes were made.



potential for applications in health detection, disease diagnosis, rehabilitation therapy, and human-machine interaction.

Keywords: Liquid metal, epidermal electrodes, health monitoring, flexible devices

INTRODUCTION

The efficient recording of epidermal electrophysiological signals and their long-term reliability are essential for health monitoring, disease diagnosis, rehabilitation therapy, and human-computer interaction^[1-3]. To enable high-quality electrophysiological recording over extended durations, bioelectrodes interfacing with soft skin tissue must meet stringent criteria, including excellent conformability, mechanical properties similar to those of biological tissues, and long-term reliability^[4,5]. However, commonly utilized metal plate electrodes and silver/silver chloride (Ag/AgCl) gel electrodes are only appropriate for short-term and static measurements due to the rigidity-flexibility disparity with soft skin, while the ion-conductive gel is susceptible to water evaporation and interference from sweat ions^[6,7]. Extensive research has been conducted on flexible electrodes that can bend and stretch to adapt to skin deformation, thereby addressing the limitations of rigid electrodes^[8]. Flexible conductive materials, including metal nanowires^[9], carbon nanotubes^[10], liquid metals^[11,12], and conductive polymers^[13], have been integrated into electrophysiological signal electrodes to ensure good conductivity. Highly elastic polymers, including silicone^[14] and polyurethane (PU)^[15], and breathable materials, including nanofibers^[16], have been utilized as electrode substrates to improve wearing comfort. Nevertheless, the human skin surface is characterized by wrinkles and depressions, exhibiting amplitudes and typical ranges of 15-100 and 40-1,000 μm , respectively^[17]. Currently, flexible electrodes are primarily planar patch-type devices that, although capable of conforming to the macroscopic contours of the skin, encounter difficulties in adapting to the microscopic textures of rough skin surfaces or densely haired regions such as the scalp, leading to gaps between the electrodes and the skin surface. These gaps diminish effective contact area, elevate electrode-skin impedance, compromise adhesion stability, and induce signal distortion during bodily movement due to electrode displacement^[18-21]. To facilitate close contact between flexible electrodes and the skin, biomimetic surface microstructures modeled after octopus tentacles^[22] and gecko feet^[23], along with adhesive materials such as polydopamine^[24] and silk fibroin^[25], have been extensively utilized in conformal electrodes to enhance skin adhesion and minimize interfacial gaps. *In situ* manufacturing techniques, including inkjet printing^[26], 3D printing^[27], stamping^[28], and direct writing with a ballpoint pen^[29], can produce conformal electrode-skin interfaces. The sensitivity of the skin to temperature and solvents necessitates that patients remain still during fabrication, and photocurable or thermally cured electrodes require additional equipment, thereby limiting the broad application of *in situ* fabricated electrodes. Consequently, developing electrophysiological signal electrodes that establish complete conformal contact with the skin for high-fidelity measurements on rough and hairy skin surfaces has become a significant challenge in this field^[30].

Liquid metals, especially gallium-based eutectic alloys characterized by high electrical conductivity, low vapor pressure, and low viscosity, have recently emerged as promising candidates for conformal bioelectronics^[31]. The liquid metal-based electrodes may conformally fill skin textures and penetrate hair under pressure, creating a fully conformal three-dimensional structure that effortlessly adapts to rough and hairy skin surfaces. The high surface energy of liquid metal leads to poor wettability on rough epidermal surfaces. Furthermore, their inherent fluidity poses challenges in preserving electrode morphology, which is easily wiped off and consequently sustains damage. Although blending liquid metal with polymers to create flexible electrodes diminishes surface tension, this approach significantly compromises the electrical conductivity.

Herein, we introduce a novel conformal electrode structure to address the challenges of achieving high conductivity and high stretchability in epidermal electrodes while simplifying complex fabrication processes. We employed semi-liquid metal (SLM), known for its excellent conductivity and fluidity, as the deformable electrode, alongside polyborosiloxane (PBS), which possesses frequency-responsive rheological properties, as the adaptable substrate. We developed an SLM with conductivity of 9.0×10^6 S/m, adjustable surface tension, and flow properties, which is subsequently coated onto a non-Newtonian fluid substrate to function as measurement electrodes. This method facilitates simultaneous optimization of conductivity and stretchability. Furthermore, the SLM electrode experiences pressure due to the slow deformation of the PBS, enhancing its skin wettability and facilitating electrode encapsulation, forming the conformal electrode. The SLM-PBS electrode exhibits exceptional skin contact with 0.1 M Ω impedance at 1,000 Hz, endures high stretching of approximately 1,000%, and retains robust adhesion for > 48 h. It can detect various epidermal bioelectrical signals, including electrocardiogram (ECG), electromyogram (EMG), and electroencephalogram (EEG), making it suitable for measurement in regions with rough textures, significant skin deformation, and dense hair coverage. It facilitates sustained dynamic monitoring of human health information, indicating extensive application prospects in health monitoring, disease diagnosis, rehabilitation therapy, and human-machine interaction.

EXPERIMENTAL

Fabrication of Cu-EGaIn

The preparation of the liquid metal started with the combination of 75.5 wt% of gallium (Anhui Minor New Materials Co., Ltd.) and 24.5 wt% of indium (Anhui Minor New Materials Co., Ltd.) in a beaker, which was then heated to 200 °C for 2 h. Subsequently, 15 wt% of silver-plated copper microparticles (15 μ m in diameter with 3 wt% Ag content, Hebei Jingrui Alloy Products Co., Ltd.) were added to the liquid metal mixture. Then, a certain amount of 1 mol/L NaOH aqueous solution was poured into the beaker. NaOH serves to remove oxides from the surfaces of liquid metal and metal particles, facilitating their fusion. After stirring for 3 min, the silver-plated copper microparticles were fully dissolved in the liquid metal, resulting in the formation of Cu-EGaIn. The fabricated SLM is rinsed with water, ensuring no NaOH residue on the surface.

Fabrication of PBS

Initially, 100 g of hydroxyl-terminated polydimethylsiloxane (PDMS) precursor (Sylgard 184, Dow Corning Inc.) and 3.03 g of boric acid (BA) ($\geq 99.5\%$, Macklin Inc.) were placed into a 250 mL three-necked flask. The mixture was stirred thoroughly for 2 h and then heated to 120 °C. Following this, the reaction was allowed to proceed for 1 h before transferring the mixture to a vacuum oven. Finally, the reaction continued for an additional 24 h at 120 °C under vacuum conditions to ensure the completion of the network formation process.

Fabrication of SLM-PBS conformal electrode

Fabrication of the electrode patch began with placing a stainless-steel template on the non-adhesive side of the PU tape. A brush, dipped in SLM, was then used to print liquid metal lines. After printing, the stainless-steel template was removed, and a circular hole with a diameter of 15 mm was cut at one end of the liquid metal lines. Then, the backing paper of the PU film was removed, allowing the PU film to adhere to the skin. Subsequently, a PBS disc with a diameter of 20 mm was fabricated, featuring a circular liquid-metal coating with a diameter of 10 mm drawn at its center. Finally, the PBS disc was placed over the circular hole of the PU tape, ensuring the edge of the circular liquid-metal coating connected to the liquid-metal lines. This setup allows the liquid-metal coating on the PBS disc to make contact with the skin through the circular hole. At the end of the liquid-metal lines, conductive tape with a width of 2 mm was attached, followed by placing another complete PU film over the initial PU film with the PBS disc.

Adhesion characterization

The PBS was applied to the surface of an Ecoflex film (10 mm × 10 mm). The other side of the PBS was adhered to the skin on the upper arm of the volunteer. The Ecoflex film was detached from the skin under three adhesion modes (Lap-shear, Pull-off, and Peeling) at varying speeds ranging from 1 to 6 mm/s. A tensile testing machine (HC-01, Dongtai Suheng Transmission Technology Co., Ltd) was used to record the adhesion force during the detachment process. A PBS sample (10 mm × 10 mm) was then applied to the upper arm skin of the subject. In the peeling mode, it was peeled off from the skin at a speed of 6 mm/s, and the maximum adhesion force during the peeling process was recorded. This PBS sample was repeatedly peeled off from the skin 50 times, with an interval of 1 min between each peel. Artificial sweat was applied to the upper arm skin of the subject to simulate the skin interface during sweating. Three groups of PBS patches (10 mm × 10 mm) were applied on the sweated areas of the upper arm. Under the three modes of lap-shear, pull-off, and peeling, these patches were detached from the skin at a speed of 6 mm/s, with the maximum adhesion force recorded during the detachment process. Additionally, three groups of PBS patches (10 mm × 10 mm) were applied to adjacent positions on the upper arm skin of the subject. A peeling experiment was conducted every 4 h at a speed of 6 mm/s, and the maximum adhesion force during the peeling process was recorded. The experiment lasted for a total of 48 h.

Electrical performance tests

Commercial Ag/AgCl electrodes, copper electrodes, and SLM-PBS conformal electrode patches were respectively attached to the arms of volunteers (30 years old, male). An electrochemical workstation (CHI760E, CH Instrument, Inc.) was utilized to measure the impedance between the electrodes and the skin over the frequency range of 1–1,000 Hz. A SLM line of 2 mm × 20 mm was drawn onto a 10 mm × 40 mm PU tape. Conductive tape was connected to both ends of the SLM wire, and then it was encapsulated with PU tape. A tensile testing machine (HC-01, Dongtai Suheng Transmission Technology Co., Ltd) was used to control the stretching rate of the SLM wire, with a stretching speed of 50 mm/s. During the uniaxial stretching and cyclic stretching tests, the resistance changes of these wires were recorded by a digital source meter (Keithley 2002, Tektronix, Inc.) following the standard four-point method. The resistances of the SLM wires with PBS and PU as substrates were measured by the source meter at different temperatures, ranging from 30 to 60 °C, controlled by a heating stage.

Body surface biosafety experiment

This study only conducted non-invasive data collection by simply placing the device on the skin, and does not involve invasive procedures or human health risks. According to Article 32 of the “Measures for the Ethical Review of Life Science and Medical Research Involving Human Subjects (Trial)”, this study meets the conditions for exemption from review. All participants participated in the experiment with informed consent. Ag/AgCl commercial electrodes, copper electrodes, and SLM conformal electrode patches, all with the same skin-contact area, were adhered to the arm skin of volunteers (30 years old, male). After 48 h, these electrodes were removed. The skin surface temperature was detected by an infrared camera (FOTRIC 220 s, Fotric Smart Technology Co., Ltd), while an optical camera was used to record the skin condition.

Cell experiments

HaCaT cells were cultured in Dulbecco's Modified Eagle Medium supplemented with 10% fetal bovine serum (FBS, Wisent Corp.) and 1% penicillin-streptomycin (PS, Thermo Fisher Scientific Inc.) for 24 h under an atmosphere of 5% CO₂ at 37 °C. PBS and SLM-PBS were added to the cell culture medium, followed by incubation at 37 °C for 45 min. Subsequently, the extracts of the materials were added to the cells in different experimental groups, and incubation was continued in an incubator for 30 min. After the incubation, the cells were washed 1–2 times. Calcein AM and propidium iodide (PI) were used to stain the cells to distinguish live cells from dead cells. The negative control group was only added with an equal

volume of medium, while the positive control group was treated with 4% paraformaldehyde (PFA) for 15 min. Finally, before taking pictures with a confocal microscope, Hoechst dye was added to stain the cell nuclei for clear observation of the nuclei during imaging. Adherent cells were detached using trypsin without ethylenediaminetetraacetic acid (EDTA) for cell collection. Cell viability and apoptosis were stained according to the protocol of the Annexin V-EGFP/PI Apoptosis Detection Kit. Specifically, 500 μ L of Binding Buffer was added and gently mixed to form a single-cell suspension. Then, 5 μ L of Annexin V-EGFP and 2 μ L of PI were added, and the mixture was incubated in the dark at room temperature for 10–20 min, followed by flow cytometry analysis. In the flow cytometer (BD AccuriTMC6 Plus, Becton, Dickinson and Company), the green fluorescence of Annexin V-EGFP was detected using the fluorescein isothiocyanate (FITC) channel (FL1), and the red fluorescence of PI was detected using the PI channel (FL3). Normal cells treated with apoptosis-inducing agents were used as a control for fluorescence compensation adjustment to eliminate spectral overlap and determine the position of the cross-gate. The negative control group was supplemented with an equal volume of medium, while the positive control group was incubated with 4% PFA for 15 min. Finally, the cell apoptosis rate was calculated.

Circuit design

A commercial ECG monitoring module (BMD101, NeuroSky Electronic Technology Co., Ltd.) was employed to acquire ECG signals. A 3D-printed enclosure was utilized to encapsulate this ECG monitoring module. The PBS electrodes outside the enclosure and the ECG monitoring module inside were interconnected through embedded copper pads. An EEG monitor was used to detect the scalp EEG of volunteers. Three PBS electrodes were applied to the forehead of the volunteer, and one PBS electrode was applied to the skin behind the ear of the volunteer. An analog front-end amplifier (ADS1298, Texas Instruments, Inc., Dallas, TX, USA) was utilized to collect EMG signals. A Bluetooth system-on-chip (nRF52832, Nordic Semiconductor Co., Ltd.) was adopted for signal processing and transmission.

RESULTS AND DISCUSSION

Figure 1A illustrates the simple double layer structure of the conformal electrode comprising a bottom SLM coating and a top PBS film. PBS was selected as the deformable substrate for the conformal electrode because of its excellent biocompatibility, biodegradability, non-toxicity, and potential for large-scale production and was synthesized through the condensation reaction of BA with hydroxyl end-blocked dimethylsiloxane. In PBS, physical cross-links through hydrogen bonds, dynamic reversible coordination bonds between boron and oxygen atoms, and topological entanglements can be formed, while its high backbone mobility and abundant hydroxyl groups confer unique adhesive properties upon contact with human skin. Additionally, SLM was synthesized by incorporating solid copper particles into liquid metal by stirring in an alkaline solution [Supplementary Figure 1]. Compared to liquid metal, SLM exhibits lower fluidity [Supplementary Figure 2] and higher electrical conductivity, reaching 9.0×10^6 S/m [Supplementary Figure 3] when compared to prior studies on conformal electronic skin, as depicted in Supplementary Figure 4. The X-ray photoelectron spectroscopy (XPS) survey spectrum reveals the presence of oxygen on the SLM surface. Within the Ga2p spectrum, two peaks corresponding to Ga0 and two peaks corresponding to Ga³⁺ are observed. The dominant peak in the O1s spectrum is located at 530.49 eV, indicating that oxygen predominantly exists within a metal oxide. Collectively, these findings indicate that Ga₂O₃ constitutes the primary surface component of the SLM [Supplementary Figure 5]. The abundant hydroxyl groups on PBS molecular chains form extensive hydrogen bonds with gallium oxide on the SLM surface, ensuring stable adhesion of SLM to PBS. This interaction facilitates simultaneous synchronous deformation of SLM and PBS on the skin, effectively addressing skin wrinkles. This unique structure provides the conformal electrode with high skin adhesion, exceptional stretchability, tolerance to skin hair, and conformal contact with the skin [Figure 1B, Supplementary Video 1]. Figure 1C depicts that a stretchable wire was further fabricated using SLM to interconnect with this conformal patch, forming an electrode system

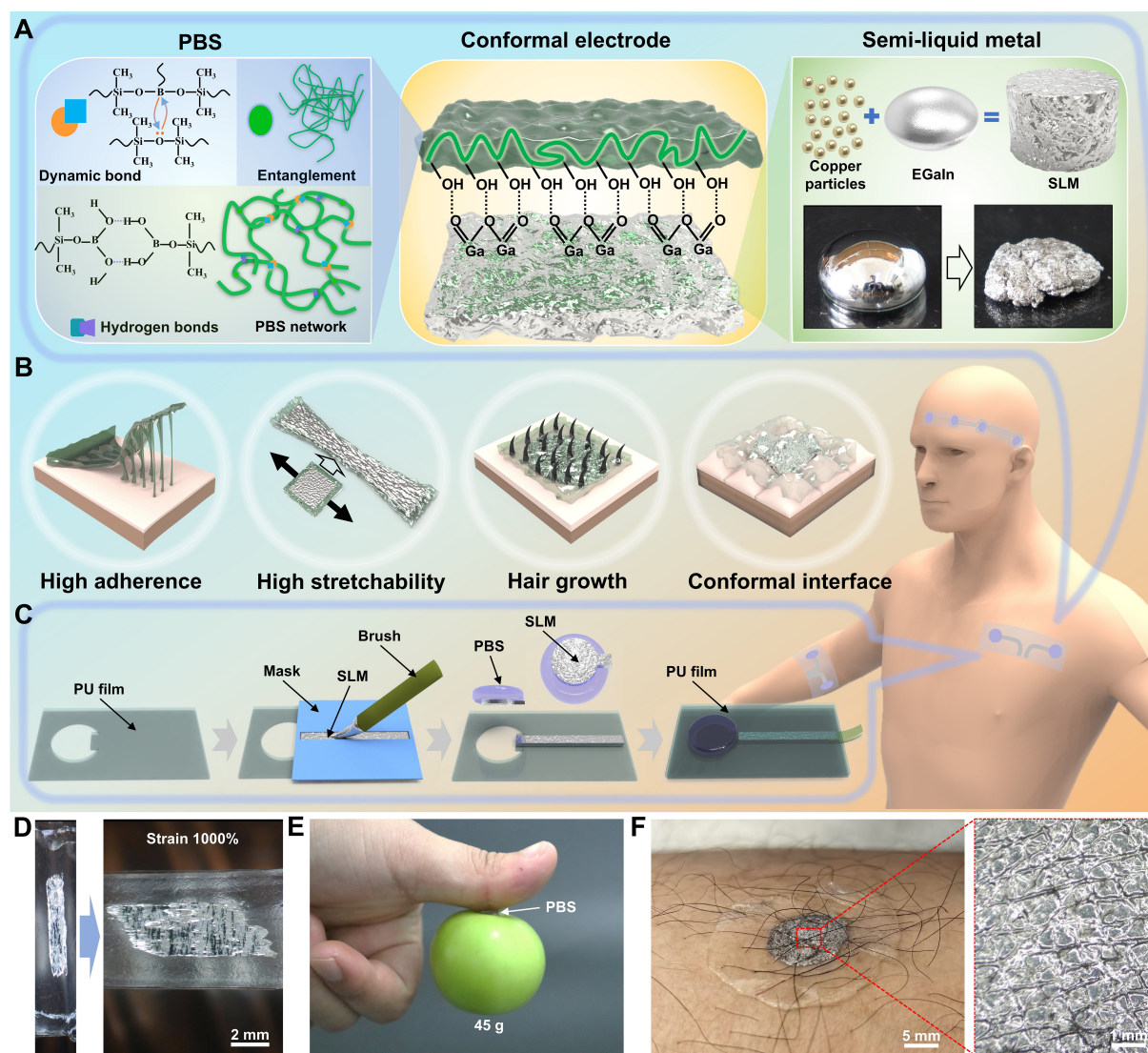


Figure 1. Material overview and multifunctional characteristics of the skin-conformal electrode. (A) Schematic of the fabrication method for SLM and PBS constituting the conformal electrode; (B) Multiple advantages of the conformal electrode; (C) Schematic of the fabrication method for the stretchable wire paired with the conformal electrode; (D) Image demonstrating the high stretchability of the conformal electrode; (E) Image demonstrating the high adhesion of PBS; (F) Images showing the conformal attachment of the electrode to human skin. SLM: Semi-liquid metal; PBS: polyborosiloxane.

[Supplementary Video 2]; the comprehensive fabrication procedure of the system is displayed in Supplementary Figure 6. Figure 1D and Supplementary Figure 7 depict the high stretchability of the double-layer structure, wherein the low fluidity of SLM ensures stable adhesion to PBS even during excessive stretching of approximately 1,000% without crack formation [Supplementary Video 3]. The PBS substrate has adequate sufficient adhesion to human skin, enabling it to attach objects of various materials, including plastic, wood, and gypsum, weighing up to 45 g to the skin [Figure 1E and Supplementary Figure 8]. SLM and PBS possess fluidity, enabling the conformal electrode to overcome hair interference and closely adhere to the surface of hairy skin, thereby facilitating high-quality surface physiological signal assessment on human skin [Figure 1F].

Benefiting from the high mobility of its backbone and abundant hydrogen bonds, PBS becomes flowable after several min of air exposure at room temperature. [Figure 2A](#) illustrates the phenomenon of rectangular-shaped PBS flowing and deforming under its weight, progressively spreading across a flat substrate. When applied to the skin, PBS expands under its pressure, enabling it to accommodate the microscopic curvature of the skin and conform to its undulating surface. Similarly, the SLM coating on PBS adheres to the microscopic curvature of skin texture during PBS compression, facilitating conformal SLM-skin contact. Replicated microscopic skin textures can be observed on PBS and SLM surfaces after peeling from the skin [[Figure 2B](#)]. The frequency-dependent rheological properties of PBS arise from the reversible cross-linking of dynamic borate bonds. Borate-containing oxane units such as $-B(OR)_2$ and $-BO_3$ on the molecular backbone or side chains covalently connect with siloxane chains $-Si-O-Si-$ through oxygen atoms, forming a dynamic $Si-O-B-O-Si$ network. With bond energies around 20-40 kJ/mol, these borate bonds undergo reversible cleavage and reformation, imparting time-dependent rheological behavior to PBS at the macroscopic scale. At room temperature, dynamic cross-linking of borate bonds forms a physical network that imparts the material with viscoelasticity. When subjected to external force or temperature stimulus, borate bonds break, leading to network disentanglement and decreased viscosity; upon removal of the stimulus, bond reformation restores viscosity. The topography contour curves of skin, PBS, and SLM show that the fingerprint depths on the three substrates are all approximately 100 μm , indicating that both the PBS and SLM coatings can closely adhere to the skin and fill the skin folds [[Supplementary Figure 9](#)]. The conformal electrodes augment the contact area with the skin and enhance the adhesive forces, including hydrogen bonds, van der Waals forces, and electrostatic forces between the skin. A series of detachment tests, including lap-shearing, pulling, and 90° peeling, were employed to quantitatively assess the interfacial adhesion between PBS and the skin. The mechanical behavior of PBS, as a non-Newtonian fluid, depends on the peeling speed; hence, the skin adhesion force was measured across a range of peeling speeds from 1-6 mm/s [[Figure 2C-E](#)]. The findings demonstrate that the adhesion force of PBS on the skin increases with the peeling speed. At a peeling speed of 1 mm/s, the adhesion forces measured in the three detachment tests were 0.4, 0.45, and 0.42 N/cm, which are adequate to ensure strong interfacial adhesion between PBS and the skin, thus facilitating excellent conformability to the skin in practical applications. Adhesion forces attain values of 1.40, 2.72, and 1.38 N/cm at 6 mm/s, indicating improved adhesion stability during rapid skin movements. Furthermore, the rheological properties of PBS facilitate its physical extraction from the skin without causing damage after the specified service duration. Besides, no leakage occurred in the SLM under both pressure and tensile states, attributed to the high adhesion between the SLM and PBS [[Supplementary Figure 10](#)]. PBS exhibits exceptional self-healing capabilities, as the replicated skin texture patterns on its surface dissipate within 25 s after detachment from the skin, allowing the electronic skin device to be utilized for several cycles [[Supplementary Figure 11](#)]. Cyclic adhesion testing at a 90° peeling angle and a speed of 6 mm/s demonstrated that adhesion exceeded 1.0 N/cm after 50 cycles, with consistent performance between 0.85 and 1.4 N/cm throughout the tests, confirming PBS reliability as an epidermal adhesive even after repeated peeling [[Figure 2F](#)]. Adhesion tests were performed under dry and wet conditions across three detachment modes. Compared to the dry conditions, PBS exhibited no significant reduction in adhesion force under wet conditions, indicating its exceptional wet adhesion capability [[Figure 2G](#)]. The peeling force of PBS was assessed after various adhesion durations, revealing a minor decrease in adhesion force from 1.4 to 1.0 N/cm after 7 days [[Figure 2H](#)], indicating excellent long-term adhesion stability on the skin and ensuring reliable surface electrophysiological signal recording over prolonged periods.

The electrical performance of the flexible, stretchable wires was assessed by testing their resistance response characteristics, cyclic stretch stability and temperature adaptability under different strains using a custom-built multifunctional mechanical-electrical coupling testing platform [[Supplementary Figure 12](#)]. The resistance of SLM wires, measuring 1.1 mm in width and 2 cm in length, exhibited significant variation

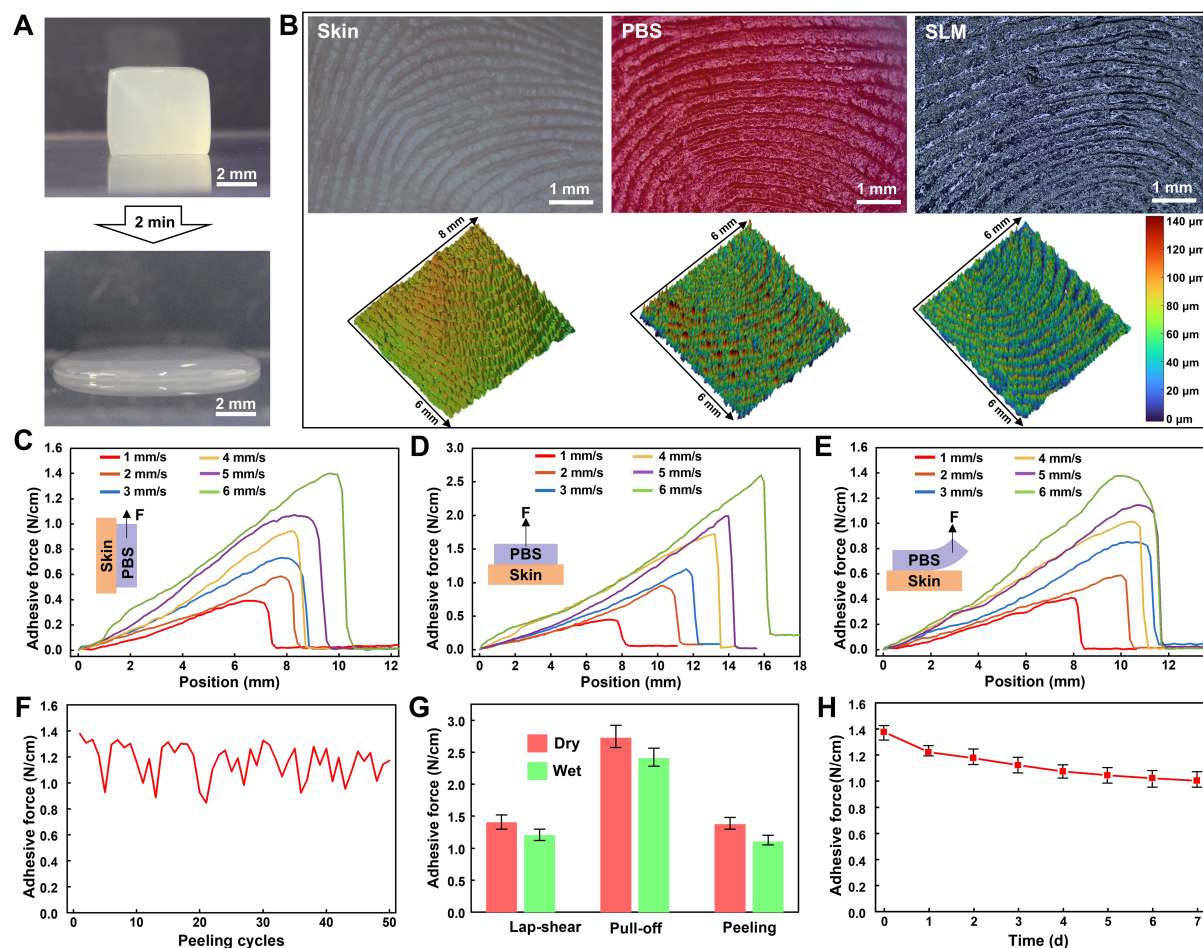


Figure 2. Adhesive characteristics of PBS. (A) The deformation of PBS under gravity within 2 min; (B) Surface microtopography of skin, PBS, and SLM; (C-E) Adhesion force-position curves between the skin and PBS patch at varying peeling speeds (1–6 mm/s); (F) Adhesion force during 50 peeling cycles; (G) Comparative bar charts illustrating adhesion force under dry/wet conditions in lap-shearing, pulling, and peeling tests; (H) Time-dependent adhesion force of PBS patch over 7 days. PBS: Polyborosiloxane; SLM: semi-liquid metal.

within the 0%-1,000% strain range, with a resistance ratio (R/R_0) reaching 19 at 1,000% strain [Figure 3A]. The resistance variations exhibited nonlinear features. In high-strain regions, resistance increased significantly due to the reconfiguration of the conductive network; however, in low-strain regions, the resistance exhibited a steady increase. Human skin can be maximally stretched to 50%-100% of its original length. Within this range, the resistance ratio of SLM wires increased to 1.16, demonstrating that the SLM stretchable wires can effectively meet the criterion for stable conductivity during the deformation of human skin. Cyclic stretching tests [Figure 3B] exhibited stable operation under strains of 50%, 100%, 200%, 280%, and 330%, with regular fluctuations in the resistance ratio affirming stability across different deformation levels. During stretching, the oxide layer thins and microcracks increase, causing resistance to rise. During recovery, the flow of liquid metal promotes crack fusion, leading to a decrease in resistance. When the number of stretching cycles is fewer than ten, the oxide layer has not suffered significant cyclic fatigue damage. Resistance changes are dominated by geometric factors such as cross-sectional area and length, resulting in consistent relative resistance changes over five consecutive stretches at the same strain state. The 5,000-cycle test at 200% strain [Figure 3C] shows the resistance ratio (R/R_0) remains between 0.9 and 1.6, demonstrating excellent long-term cyclic stability. Initially, R/R_0 decreases to 0.98 due to rearrangement of

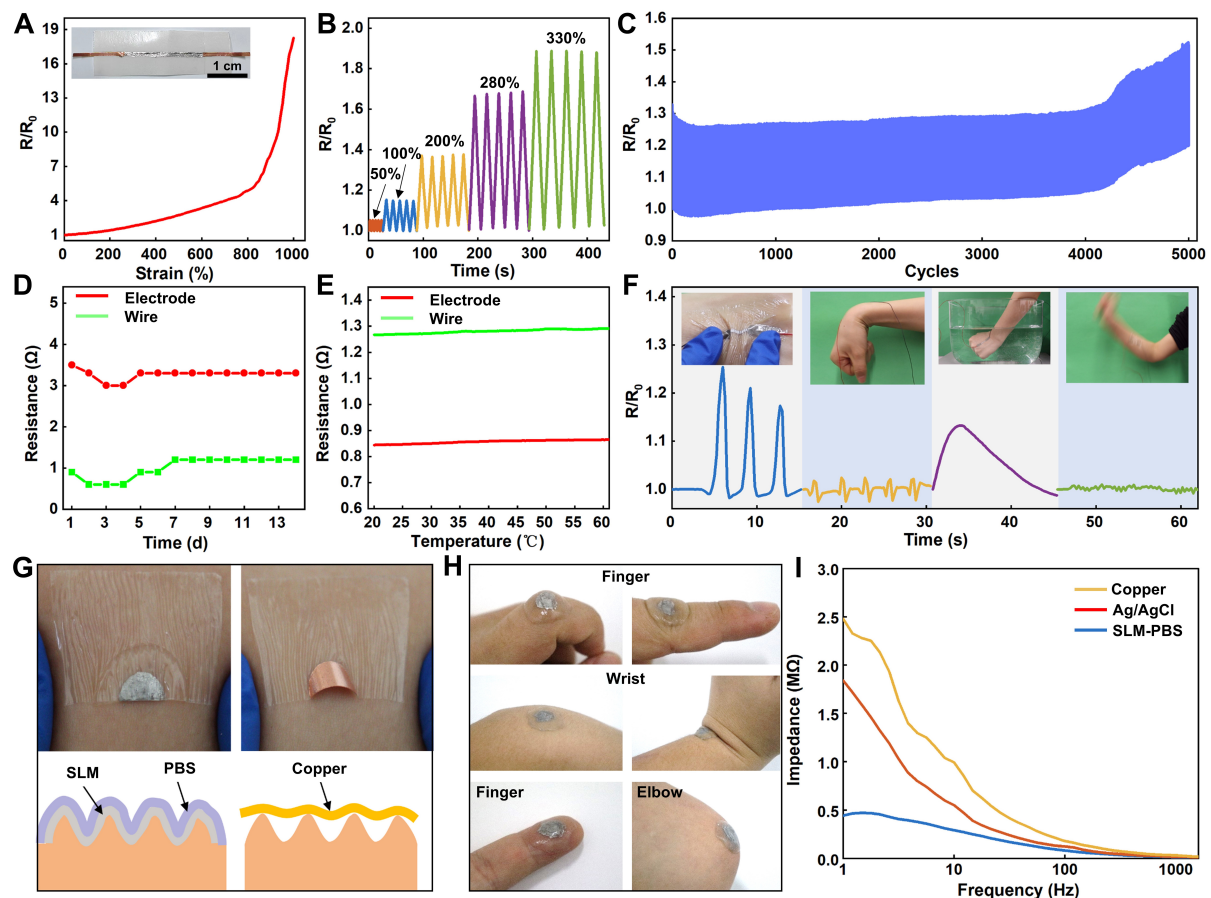


Figure 3. Electrical performance of conformal electrodes and flexible stretchable wires. (A) The image of a flexible stretchable wire and its strain-resistance variation rate (R/R_0) curve; (B) Time-dependent resistance ratio of the wire under strain amplitudes varying from 50% to 330%; (C) Resistance ratio of the wire during 5,000 stretching cycles; (D) Long-term resistance monitoring of the conformal electrodes and stretchable wires; (E) Temperature-dependent resistance variations of the conformal electrodes and stretchable wires; (F) Resistance ratio variations of the stretchable wire and images of corresponding motions; (G) Images and schematics comparing skin attachment of the conformal electrodes with copper electrodes; (H) Images of the conformal electrodes adhered to human joints and fingers; (I) Impedance-frequency characteristics of the conformal electrodes compared to copper and Ag/AgCl electrodes.

solid metal particles in the brush-coated liquid metal wire, then slowly rises. After 4,000 cycles, unrepaired cracks accumulate and resistance increases rapidly, preventing recovery to the initial state. Long-term resistance monitoring over 14 days [Figure 3D] indicated stable resistance of SLM-PBS electrodes at 3–3.5 Ω and PU-based wires at 0.5–1.2 Ω without significant fluctuations observed in either system. This illustrates the electrical stability of the material system during prolonged operation, ensuring reliable performance for long-term wearable device applications. Experiments on temperature-dependent resistance variations of wires and electrodes [Figure 3E] revealed that SLM-PBS electrodes sustained a constant resistance (0.8–0.9 Ω) between 30–60 $^{\circ}\text{C}$, but PU-based wires exhibited resistance within 1.2–1.3 Ω . Both systems exhibited low-temperature coefficients, demonstrating insensitivity to body temperature ranges and ambient thermal fluctuations, which aligns well with the physiological requirements for epidermal applications. The adhesion durability of stretchable wires and conformal electrodes on human skin was further assessed, demonstrating that the resistance of SLM wires adhered to the skin exhibited minimal changes even under skin abrasion, flexion, water immersion, or severe agitation conditions. During rubbing or compression, the maximum resistance ratio increased marginally to 1.25 [Figure 3F]. Figure 3G illustrates that the unique SLM-PBS composite structure of the conformal electrodes facilitated conformal attachment to the skin, yielding

enhanced interface contact quality compared to traditional copper electrodes. Besides, the conformal electrodes affixed to human joints exhibited robust adhesion while adapting to various bending deformations [Figure 3H]. Impedance assessments revealed that the conformal electrodes exhibited significantly lower impedance than copper and Ag/AgCl electrodes across a frequency spectrum of 1–1,000 Hz, with an impedance of 0.45 M Ω at 1 Hz diminishing to 0.1 M Ω at 1,000 Hz, indicating their enhanced signal transmission efficacy [Figure 3I]. To investigate the effects of external environmental factors on electrode performance, we measured the impedance of SLM-PBS electrodes under humidity levels and different temperatures [Supplementary Figure 13]. The results show that the skin contact impedance of the SLM-PBS electrodes decreases with increasing temperature. For example, at 17 °C, the impedance at 10 Hz is 47.5 k Ω , whereas it decreases to 20.3 k Ω at 65 °C. This behavior may be attributed to the partial breaking of borate bonds within the PBS network at elevated temperatures, which enhances polymer chain mobility and softens the material, thus promoting better conformity with the skin microstructure and increasing the effective contact area. Additionally, higher temperatures improve skin surface hydration, further facilitating the formation of a better electrical contact interface between the electrode and the skin. Tests under different humidity levels revealed that at 38% humidity, the impedance at 10 Hz is 53.3 k Ω , decreasing to 24.7 k Ω at 90% humidity. This trend can be explained by the combined effects of humidity on the electrode material structure and the hydration layer on the skin surface. SLM-PBS electrodes exhibited enhanced long-term electrical stability, with minimal impedance variations after 24 h [Supplementary Figure 14], facilitating reliable prolonged electrophysiological signal recording. This flexible, stretchable wire and conformal electrode exhibit exceptional electrical performance characterized by significant strain response, cyclical stability, long-term durability, temperature adaptability, and physiological signal acquisition, with their structural design and material system ensuring electrical stability suitable for human skin applications.

The biocompatibility of PBS and SLM-PBS electrodes has been examined through cytotoxicity assessments and skin irritation tests. The biocompatibility of PBS and SLM-PBS electrodes was assessed through co-culture experiments with human immortalized keratinocytes (HaCaT) cells. Initially, PBS and PBS-SLM were incubated in a cell culture medium at 37 °C for 45 min, after which their extracts were added to HaCaT cells for an additional 30 min before conducting a cytotoxicity evaluation. Confocal microscopy images [Figure 4A] demonstrated robust strong and homogenous green fluorescence in HaCaT cells treated with PBS and PBS-SLM, consistent with the cellular condition observed in the blank group cultured in a normal medium. Conversely, the 4% PFA-treated positive control group exhibited red fluorescence from PI staining in dead cells; however, no significant red fluorescence was observed in the cells treated with PBS and SLM-PBS, indicating a lack of cell death. Figure 4B depicts that cell viability for PBS and SLM-PBS treatments exceeded 95%, confirming their non-cytotoxicity and excellent biosafety. Cell health is not solely described by viability; cell vitality is also a critical indicator for evaluating material safety. Cell viability can be assessed through apoptosis assays, which yield indicators of cell death markers, including the loss of membrane integrity. Flow cytometry was utilized to analyze HaCaT cell apoptosis rates, further confirming the cellular safety of PBS and SLM-PBS. Supplementary Figure 15 displays that the Q4 quadrant (viable cells) proportions for the blank control, PBS, and PBS-SLM groups were 98.1%, 96.4%, and 96.4%, respectively, consistent with the cell viability results (> 95%) from the fluorescence microplate reader. This signifies that PBS and SLM-PBS groups preserved cell viability comparable to the blank control. Furthermore, the Q3 quadrant (early apoptotic cells) proportions for PBS and PBS-SLM groups were significantly lower than those of the 4% PFA positive control, indicating minimal impact on HaCaT cell activity. Similarly, the Q2 quadrant (dead cells) proportions in the positive control were substantially higher than those in PBS and PBS-SLM groups, confirming no significant apoptosis induction by these materials. The cytotoxicity and vitality-related experiments collectively demonstrate the favorable cellular safety of PBS and SLM-PBS materials. The SLM-PBS electrode, copper electrode, and Ag/AgCl electrode were

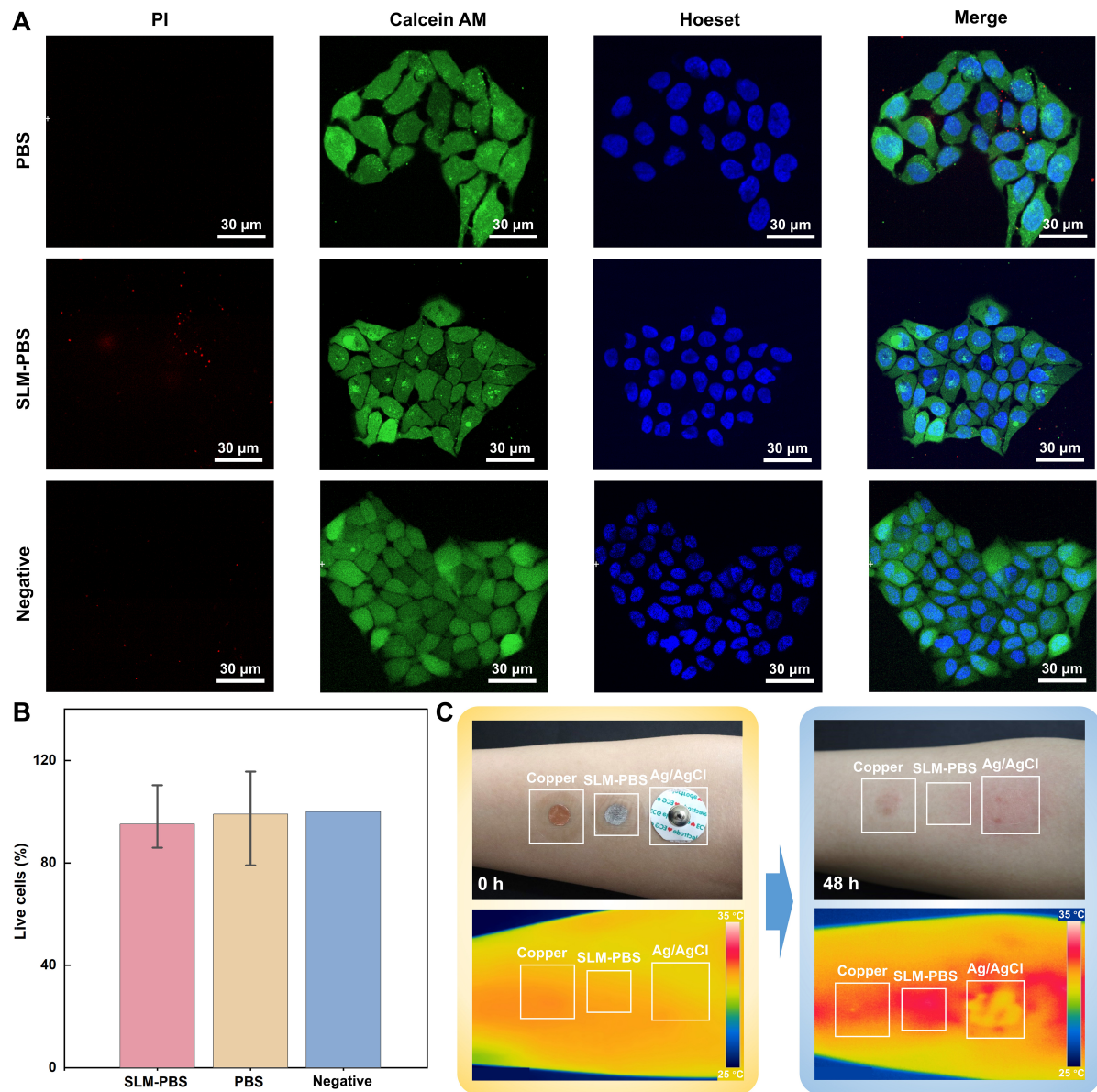


Figure 4. Biosafety evaluation results of SLM-PBS materials. (A) Fluorescence staining images of cells in the PBS group, SLM-PBS group, and negative control group, showing PI, Calcein AM, Hoechst staining, and merged images; (B) Statistical bar chart of cell viability for SLM-PBS group, PBS group, and negative control group; (C) Comparative images of visual observation and infrared thermography for a copper electrode, a SLM-PBS electrode, and an Ag/AgCl electrode adhered to skin at 0 and 48 h. SLM: Semi-liquid metal; PBS: polyborosiloxane; PI: propidium iodide.

simultaneously affixed to human skin for 48 h to compare their biocompatibility [Figure 4C]. Visual inspection revealed no irritation, including redness, swelling, or allergic reactions on skin areas beneath SLM-PBS electrodes. Conversely, mild redness was observed under copper electrodes, indicating reduced skin irritation by SLM-PBS materials. Infrared thermography exhibited stable skin temperatures between 33 and 35 °C under SLM-PBS electrodes, without abnormal thermal fluctuations compared to copper and Ag/AgCl electrodes, confirming their temperature adaptability and safe epidermal integration. From cellular to *in vivo* levels, SLM-PBS materials exhibit exceptional biosafety, validating their practical potential for wearable epidermal electrodes and adherence to long-term medical monitoring device requirements.

The SLM-PBS electrode was initially employed for ECG signal acquisition under static and dynamic conditions to assess its capability for monitoring physiological electrical signals on the body surface. [Figure 5A](#) depicts that the SLM-PBS electrode was affixed to the chest skin surface using an integrated device that included a PU film, Cu-EGaln wires, the SLM-PBS electrode, a pad, a printed circuit board (PCB), and two shells. The findings indicate that the SLM-PBS electrode and conventional Ag/AgCl electrodes effectively captured ECG waveform features, including P waves, QRS complexes, and T waves, exhibiting strong morphological consistency [[Figure 5B](#)]. The enhanced local waveforms demonstrated that the SLM-PBS electrode achieved accuracy in detecting the QRS complex similar to that of the Ag/AgCl electrode, with peak amplitudes and interval errors remaining within acceptable ranges. Despite the impacts of electrode polarization, surface oxidation, and interfacial capacitance, the SLM-PBS electrode exhibited a signal-to-noise ratio (SNR) of 18.20 dB. This is only 1.58 dB lower than 19.78 dB of the Ag/AgCl electrode [[Supplementary Figure 16](#)], demonstrating comparable ECG signal acquisition quality to traditional medical electrodes and validating its signal transmission reliability. The thickness of the SLM coating was controlled by the number of brush coating times. [Supplementary Figure 17](#) shows that the thickness of the electrode does not affect the measurement of ECG signals. [Figure 5C](#) illustrates the heart rate variability curve recorded by SLM-PBS electrodes over 1 h, during which the heart rate exhibited dynamic fluctuations between 60 and 90 beats per min, accurately reflecting changes in cardiac rhythm. [Figure 5D](#) depicts that the scatter plots of the R-R intervals illustrate that the intervals range from 600 to 1,100 ms, with the scatter pattern closely corresponding to the physiological attributes of human cardiac rhythms. This further substantiates the accuracy of SLM-PBS electrodes in recording temporal ECG signal features, establishing a solid basis for heart rate variability analysis. Subsequently, SLM-PBS electrodes were employed in typical daily scenarios to validate their ECG signal monitoring capabilities across different activity stages. The results indicate that the SLM-PBS electrodes can reliably capture ECG signals under static conditions, including standing, lying, and working, and dynamic conditions, including walking and running [[Figure 5E](#)]. Under static conditions, the acquired waveforms remain regular with low noise levels. During dynamic activities, despite motion-induced noise interference, the electrodes consistently maintain clear QRS complexes without signal loss or waveform distortion. The periodic fluctuations caused by breathing movements, including variations in skin-electrode contact impedance, thoracic impedance changes, and minor cardiac positional shifts, can be effectively reduced through data processing methods such as filtering. These methods preserve the accurate detection and analysis of key ECG characteristics such as waveform morphology and peak positions [[Supplementary Figure 18](#)].

The SNRs of ECG signals obtained under these conditions were measured at 15.38, 19.73, 17.02, 16.28, and 13.9 dB [[Supplementary Figure 19](#)], meeting clinical electrode standards. This confirms the superior motion adaptability of the SLM-PBS electrodes, satisfying ECG monitoring requirements during daily activities and exercise, and exceeding conventional rigid electrodes in dynamic environments. This study demonstrated that liquid metal-based SLM-PBS conformal electrodes exhibit exceptional performance in human ECG monitoring. They achieve high-fidelity signal acquisition under static and dynamic conditions, offering an innovative solution for wearable ECG devices. Their collective advantages in biocompatibility, signal stability, and motion adaptability render them promising instruments for portable medical monitoring and sports health management applications.

High-quality EEG recordings are essential for clinical and research-based neurological applications, including neurodisorder diagnosis and brain-machine interfaces (BMIs), as EEG provides an effective, non-invasive method to monitor brain electrical activity with precise temporal resolution. Leveraging the fluidity of PBS, SLM-PBS electrodes can attain superior conformal adherence to a hairy scalp, facilitating high-fidelity EEG acquisition. SLM-PBS electrodes were utilized at FP1, FP2, and FPZ positions for EEG

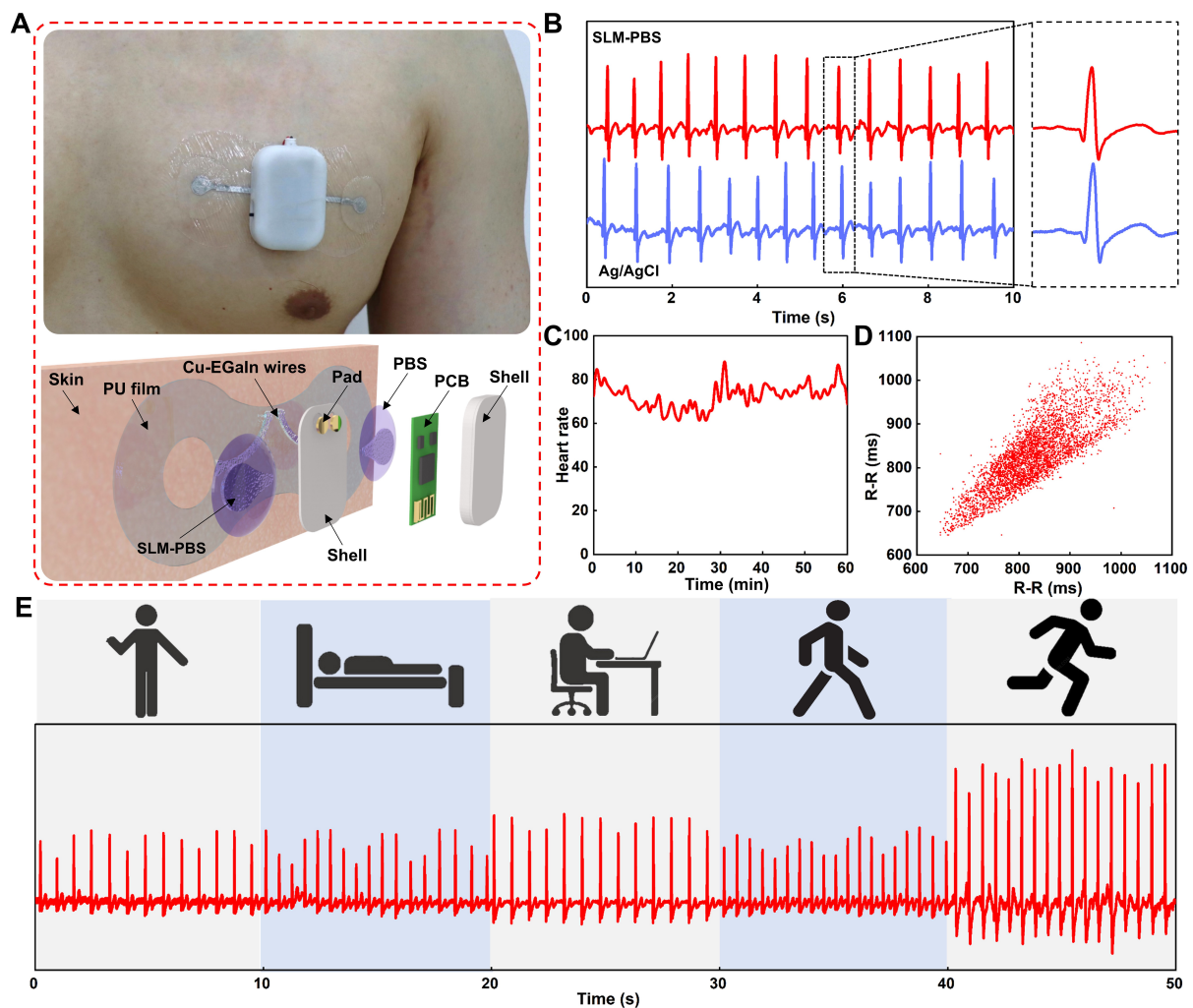


Figure 5. Performance characterization of human ECG monitoring using the SLM-PBS electrodes. (A) Image and schematic of the flexible ECG monitoring device; (B) Comparative ECG signals acquired by the SLM-PBS electrodes and Ag/AgCl electrodes; (C) Heart rate variability monitored by the SLM-PBS electrodes; (D) Scatter plot distribution of R-R intervals in ECG signals collected by the SLM-PBS electrodes; (E) ECG signals recorded by the SLM-PBS electrodes under multi-scenario conditions including standing, lying, working, walking, and running. ECG: Electrocardiogram; SLM: semi-liquid metal; PBS: polyborosiloxane.

recording as a proof-of-concept [Figure 6A]. The comparative impedance measurement of SLM-PBS electrodes and Ag/AgCl electrodes [Figure 6B] revealed that the SLM-PBS electrode exhibited an impedance of 22 k Ω at the FP1 position, significantly lower than the 68 k Ω of the Ag/AgCl electrode. At the FP2 position, the impedance of the SLM-PBS electrode was 12 k Ω , merely one-fourth of the 52 k Ω of the Ag/AgCl electrode. Similarly, at the FPZ position, the SLM-PBS electrode impedance was significantly reduced at 8 k Ω compared to the 40 k Ω of the Ag/AgCl electrode. The low impedance characteristics enhance skin-electrode contact for SLM-PBS electrodes, ensuring consistent EEG signal acquisition. Figure 6C illustrates EEG signals and their power spectral density (PSD) obtained from FP1, FP2, and FPZ positions. The EEG time-domain waveforms displayed signal fluctuations within $-40\sim 40\ \mu\text{V}$, with distinct features and minimal noise interference. PSD analysis revealed that signal energy predominantly concentrated in the 0-25 Hz frequency band, consistent with the physiological features of EEG signals. These findings validate the high-quality signal acquisition proficiency of SLM-PBS electrodes across various EEG positions, satisfying the precision criteria for EEG signal analysis.

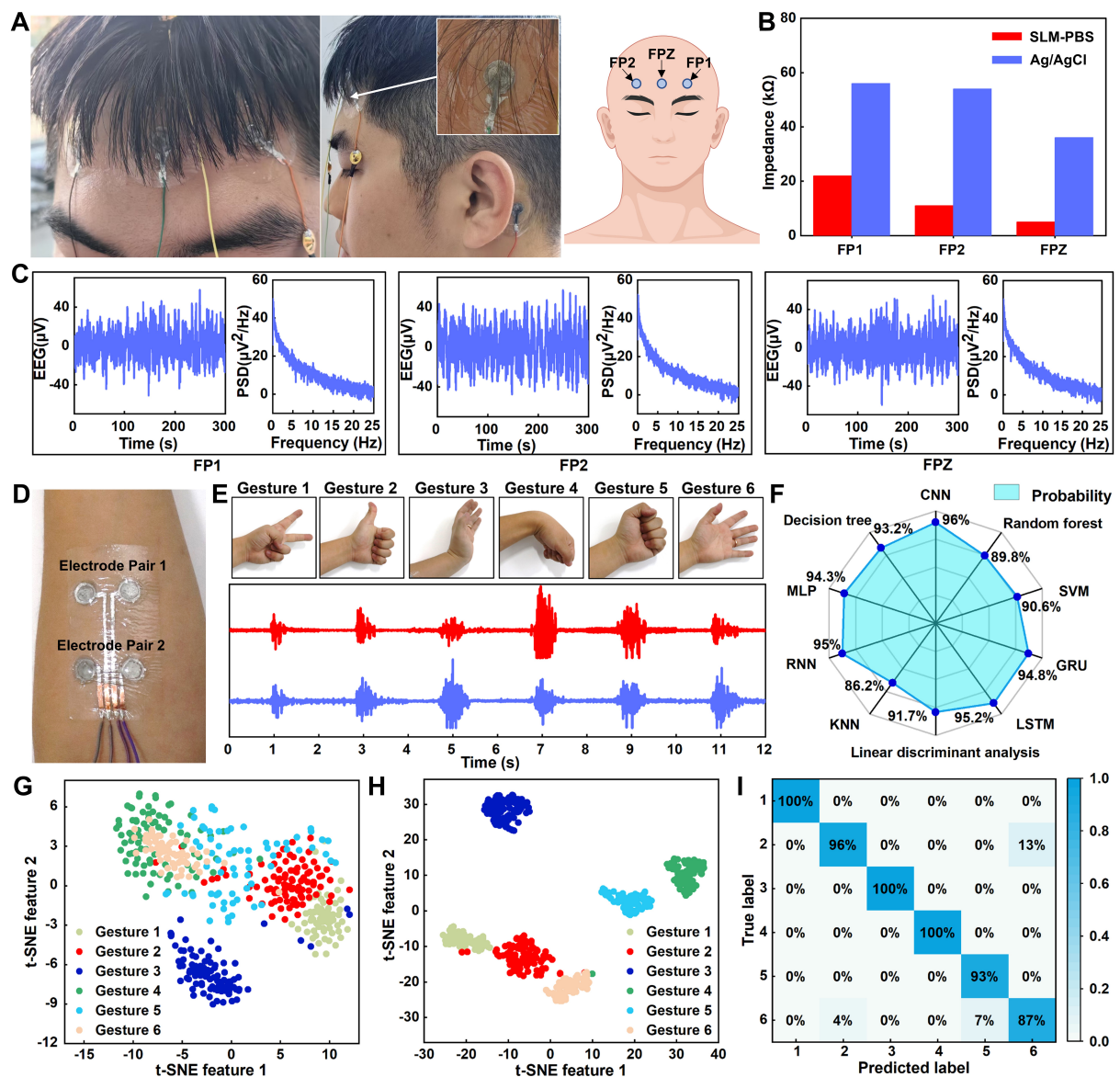


Figure 6. Performance characterization of human EEG and EMG signal monitoring and gesture recognition using SLM-PBS electrodes. (A) Images of SLM-PBS flexible electrodes attached to the scalp for EEG acquisition, close-up view, and the schematic of EEG positions including FP1, FP2, FPZ; (B) Impedance comparison chart between SLM-PBS electrodes and Ag/AgCl electrodes at FP1, FP2, and FPZ positions; (C) EEG time-domain waveforms and corresponding PSD plots at FP1, FP2, and FPZ positions; (D) Image of SLM-PBS electrodes attached to the forearm for EMG acquisition; (E) Schematics of six hand gestures and corresponding EMG time-domain waveforms; (F) Radar chart comparing gesture recognition accuracies of multiple machine learning algorithms; (G and H) The t-SNE dimensionality reduction visualizations of EMG signal features for six hand gestures; (I) Confusion matrix of CNN-based gesture recognition results. EEG: Electroencephalogram; EMG: electromyogram; SLM: semi-liquid metal; PBS: polyborosiloxane; PSD: power spectral density; t-SNE: t-distributed stochastic neighbor embedding; CNN: convolutional neural network.

Figure 6D presents SLM-PBS flexible electrodes affixed to the human forearm to establish a dual-channel EMG acquisition system. The SLM-PBS electrodes effectively captured the appropriate EMG signal variations for six distinct hand gestures [Figure 6E]. The time-domain waveforms exhibited significant differences in amplitude and frequency across gestures, providing rich features for subsequent gesture recognition. Participants successively performed six gestures; each repeated 100 times with 2 s intervals. Supplementary Figures 20 and 21 present the EMG signals of the six gestures recorded by Channel 1 and

Channel 2, respectively. To eliminate the effects of muscle conditions and individual differences, improve classification accuracy, and expand its application potential in smart prosthetics, intelligent gloves, and brain-computer interfaces, multiple machine learning algorithms were employed for gesture recognition [Figure 6F]. The decision tree attained an accuracy of 93.2%, the random forest achieved 89.8%, the support vector machine (SVM) attained 90.8%, while the convolutional neural network (CNN) recorded the highest accuracy of 96%. Sequential models, including the recurrent neural network (RNN), gated recurrent unit (GRU), and long short-term memory (LSTM), achieved accuracies of 86.2%, 94.8%, and 95.2%, respectively. Linear discriminant analysis (LDA) and k-nearest neighbors (KNN) achieved accuracies of 94.3% and 91.7%, respectively. Consequently, CNN was identified as the optimal algorithm for utilizing EMG signals obtained from SLM-PBS electrodes for gesture recognition. The features of six gesture types were subsequently visualized using the t-SNE dimensionality reduction algorithm [Figure 6G and H]. In Figure 6G, scatter points of different colors denote distinct gesture categories, indicating strong intra-class clustering and inter-class separation. Figure 6H provides further details on feature distributions, where Gestures 1-6 formed independent clusters, confirming EMG features effectively characterize different gestures. The final confusion matrix [Figure 6I] demonstrated CNN recognition accuracies of 100%, 96%, 100%, 100%, 93%, and 87% for Gestures 1-6, respectively, proving high-precision recognition using SLM-PBS electrodes combined with CNN.

The SLM-PBS conformal electrode exhibits numerous advantages in EEG and EMG signal monitoring. In EEG monitoring, its low impedance properties and high-quality signal acquisition capability exceed those of conventional Ag/AgCl electrodes. In EMG monitoring, dual-channel signal acquisition comprehensively retains gesture characteristics, facilitating efficient gesture recognition when integrated with CNN algorithms. The flexibility and stretchability of SLM-PBS electrodes ensure stable adhesion to complex body surfaces, including the head and forearm, thus ensuring consistent and precise signal acquisition. This technique advances EEG research with high-quality signal collection and supports EMG-driven human-machine interaction systems, including prosthetic control and smart home interfaces.

CONCLUSIONS

This study developed a novel conformal bioelectrode system utilizing SLM and PBS, effectively overcoming the primary limitations of conventional rigid electrodes, including skin-electrode interface mismatch, inadequate adhesion, and insufficient stretchability. Through material design and structural innovation, the electrode attains high conformal contact with skin and ensures stable bioelectrical signal recording, offering a new paradigm for wearable health monitoring devices. Despite significant advancements, further optimizations are necessary. Increasing wire width and employing nitrogen protection can help minimize oxide layer formation. Additionally, the long-term stability of the SLM-PBS interface during cyclic loading requires validation, and the mechanical modulus of PBS can be optimized through molecular design to better match that of the skin, thus enhancing wearing comfort. The usage thresholds of SLM-PBS electrodes on skin with varying hair density and roughness require further quantitative definition. Moreover, removal methods for electrodes applied to high-density, long-haired areas still need improvement. Future work should focus on integrating multimodal sensors, including simultaneous temperature and humidity monitoring, and developing wireless transmission modules to enhance applications in telemedicine and rehabilitation training. This study presents an innovative solution for epidermal electronics that combines high conductivity, robust adhesion, and biocompatibility. The SLM-PBS conformal electrode system possesses significant potential in health monitoring, disease diagnosis, and human-machine interaction. The material design philosophy offers essential insights for flexible bioelectronic devices, advancing wearable technologies to better align with human physiological requirements.

DECLARATIONS

Authors' contributions

Conceptualization: Guo, R.; Fan, H.

Investigation: Liu, X.; Wan, C.; Liu, J. (Jiaping Liu); Xu, H.; Liu, Y. (Yanqing Liu)

Visualization: Guo, R.; Liu, X.; Liu, J. (Jiaping Liu); Liu, Y. (Yubing Liu); Liu, Y. (Yi Liu)

Funding acquisition: Guo, R.; Wan, C.

Supervision: Guo, R.; Fan, H.; Liu, J. (Jing Liu)

Writing - original draft: Guo, R.; Liu, X.

Writing - review and editing: Guo, R.; Liu, X.; Wan, C.; Wang, H.

Availability of data and materials

The authors declare that the primary data supporting the findings of this study are available within the paper and its [Supplementary Materials](#). Additional data are available from the corresponding authors upon reasonable request.

Financial support and sponsorship

This work is supported by the National Natural Science Foundation of China (Grant No. 62304150), China Postdoctoral Science Foundation (Grant No. 2024M753315), and Opening Project of the Key Laboratory of Bionic Engineering, Jilin University.

Conflicts of interest

All authors declared that there are no conflict of interest.

Ethical approval and consent to participate

This study only conducted non-invasive data collection through simply placing the device on the skin, and does not involve invasive procedures or human health risks. According to Article 32 of the “Measures for the Ethical Review of Life Science and Medical Research Involving Human Subjects (Trial)”, this study meets the conditions for exemption from review. All participants participated in the experiment with informed consent.

Consent for publication

The use of the photos has been obtained with the participants' informed consent for publication.

Copyright

© The Author(s) 2025.

REFERENCES

1. Wang, W.; Zhou, H.; Xu, Z.; Li, Z.; Zhang, L.; Wan, P. Flexible conformally bioadhesive MXene hydrogel electronics for machine learning-facilitated human-interactive sensing. *Adv. Mater.* **2024**, *36*, e2401035. [DOI PubMed](#)
2. Hu, H.; Huang, H.; Li, M.; et al. A wearable cardiac ultrasound imager. *Nature* **2023**, *613*, 667-75. [DOI PubMed PMC](#)
3. Xia, M.; Liu, J.; Kim, B. J.; et al. Kirigami-structured, low-impedance, and skin-conformal electronics for long-term biopotential monitoring and human-machine interfaces. *Adv. Sci.* **2024**, *11*, e2304871. [DOI PubMed PMC](#)
4. Lo, L. W.; Zhao, J.; Aono, K.; et al. Stretchable sponge electrodes for long-term and motion-artifact-tolerant recording of high-quality electrophysiologic signals. *ACS. Nano.* **2022**, *16*, 11792-801. [DOI PubMed PMC](#)
5. Li, J.; Ma, Y.; Huang, D.; et al. High-performance flexible microneedle array as a low-impedance surface biopotential dry electrode for wearable electrophysiological recording and polysomnography. *Nanomicro. Lett.* **2022**, *14*, 132. [DOI PubMed PMC](#)
6. Pan, S.; Zhang, F.; Cai, P.; et al. Mechanically interlocked hydrogel-elastomer hybrids for on-skin electronics. *Adv. Funct. Mater.* **2020**, *30*, 1909540. [DOI](#)
7. Yuk, H.; Lu, B.; Zhao, X. Hydrogel bioelectronics. *Chem. Soc. Rev.* **2019**, *48*, 1642-67. [DOI PubMed](#)

8. Liu, K.; Duan, T.; Zhang, F.; et al. Flexible electrode materials for emerging electronics: materials, fabrication and applications. *J. Mater. Chem. A*. **2024**, *12*, 20606-37. [DOI](#)
9. Ding, Y.; Xiong, S.; Sun, L.; et al. Metal nanowire-based transparent electrode for flexible and stretchable optoelectronic devices. *Chem. Soc. Rev.* **2024**, *53*, 7784-827. [DOI](#)
10. Jang, W.; Kim, B. G.; Seo, S.; et al. Strong dark current suppression in flexible organic photodetectors by carbon nanotube transparent electrodes. *Nano. Today*. **2021**, *37*, 101081. [DOI](#)
11. Guo, R.; Li, X.; Zhou, Y.; et al. Semi-liquid metal-based highly permeable and adhesive electronic skin inspired by spider web. *Sci. Bull.* **2024**, *69*, 2723-34. [DOI](#)
12. Xu, Y.; Su, Y.; Xu, X.; et al. Porous liquid metal-elastomer composites with high leakage resistance and antimicrobial property for skin-interfaced bioelectronics. *Sci. Adv.* **2023**, *9*, eadf0575. [DOI](#) [PubMed](#) [PMC](#)
13. Dimov, I. B.; Sautter, A.; Lövenich, W.; Neumann, C.; Malliaras, G. G. Adhesive cutaneous conducting polymer electrodes. *Appl. Phys. Rev.* **2022**, *9*, 021401. [DOI](#)
14. Maithani, Y.; Choudhuri, B.; Mehta, B.; Singh, J. Self-adhesive, stretchable, and dry silver nanorods embedded polydimethylsiloxane biopotential electrodes for electrocardiography. *Sens. Actuators. A. Phys.* **2021**, *332*, 113068. [DOI](#)
15. Luo, G.; Xie, J.; Liu, J.; et al. Highly conductive, stretchable, durable, breathable electrodes based on electrospun polyurethane mats superficially decorated with carbon nanotubes for multifunctional wearable electronics. *Chem. Eng. J.* **2023**, *451*, 138549. [DOI](#)
16. Zheng, S.; Wang, X.; Li, W.; Liu, Z.; Li, Q.; Yan, F. Pressure-stamped stretchable electronics using a nanofibre membrane containing semi-embedded liquid metal particles. *Nat. Electron.* **2024**, *7*, 576-85. [DOI](#)
17. Kim, D. H.; Lu, N.; Ma, R.; et al. Epidermal electronics. *Science* **2011**, *333*, 838-43. [DOI](#) [PubMed](#)
18. Sang, S.; Pei, Z.; Zhang, F.; et al. Three-dimensional printed bimodal electronic skin with high resolution and breathability for hair growth. *ACS Appl. Mater. Interfaces*. **2022**, *14*, 31493-501. [DOI](#)
19. Tian, Q.; Zhao, H.; Wang, X.; et al. Hairy-skin-adaptive viscoelastic dry electrodes for long-term electrophysiological monitoring. *Adv. Mater.* **2023**, *35*, e2211236. [DOI](#) [PubMed](#)
20. Wang, C.; Wang, H.; Wang, B.; et al. On-skin paintable biogel for long-term high-fidelity electroencephalogram recording. *Sci. Adv.* **2022**, *8*, eabo1396. [DOI](#) [PubMed](#) [PMC](#)
21. Ferrari, L. M.; Sudha, S.; Tarantino, S.; et al. Ultraconformable temporary tattoo electrodes for electrophysiology. *Adv. Sci.* **2018**, *5*, 1700771. [DOI](#) [PubMed](#) [PMC](#)
22. Kim, D. W.; Kim, H.; Hwang, G.; et al. Conformably skin-adherent piezoelectric patch with bioinspired hierarchically arrayed microsuckers enables physical energy amplification. *ACS. Energy. Lett.* **2022**, *7*, 1820-7. [DOI](#)
23. Ma, Y.; Ma, S.; Wu, Y.; et al. Remote control over underwater dynamic attachment/detachment and locomotion. *Adv. Mater.* **2018**, *30*, e1801595. [DOI](#) [PubMed](#)
24. Gan, D.; Huang, Z.; Wang, X.; et al. Bioadhesive and electroactive hydrogels for flexible bioelectronics and supercapacitors enabled by a redox-active core-shell PEDOT@PZIF-71 system. *Mater. Horiz.* **2023**, *10*, 2169-80. [DOI](#) [PubMed](#)
25. Huang, J.; Wang, L.; Jin, Y.; et al. Tuning the rigidity of silk fibroin for the transfer of highly stretchable electronics. *Adv. Funct. Mater.* **2020**, *30*, 2001518. [DOI](#)
26. Bhat, K. S.; Ahmad, R.; Wang, Y.; Hahn, Y. Low-temperature sintering of highly conductive silver ink for flexible electronics. *J. Mater. Chem. C*. **2016**, *4*, 8522-7. [DOI](#)
27. Wei, H.; Cauchy, X.; Navas, I. O.; et al. Direct 3D printing of hybrid nanofiber-based nanocomposites for highly conductive and shape memory applications. *ACS Appl. Mater. Interfaces*. **2019**, *11*, 24523-32. [DOI](#) [PubMed](#)
28. Park, J. E.; Kang, H. S.; Koo, M.; Park, C. Autonomous surface reconciliation of a liquid-metal conductor micropatterned on a deformable hydrogel. *Adv. Mater.* **2020**, *32*, e2002178. [DOI](#) [PubMed](#)
29. Chen, J. X. M.; Chen, T.; Zhang, Y.; et al. Conductive bio-based hydrogel for wearable electrodes via direct ink writing on skin. *Adv. Funct. Mater.* **2024**, *34*, 2403721. [DOI](#)
30. Huang, Y.; Wu, H.; Xiao, L.; et al. Assembly and applications of 3D conformal electronics on curvilinear surfaces. *Mater. Horiz.* **2019**, *6*, 642-83. [DOI](#)
31. Yang, J.; Cheng, W.; Kalantar-Zadeh, K. Electronic skins based on liquid metals. *Proc. IEEE*. **2019**, *107*, 2168-84. [DOI](#)